Uncovering the structural origin of shear banding in metallic glasses via tracing back to the critical glass transition process

Yu-Nuo Zhou,[1,2,*] Zeng-Yu Yang,[3,*] and Lan-Hong Dai[1,2,4,†]

[1]*State Key Laboratory of Nonlinear Mechanics, Institute of Mechanics, Chinese Academy of Sciences, Beijing 100190, China*
[2]*School of Engineering Science, University of Chinese Academy of Sciences, Beijing 100049, China*
[3]*Institute of Fluid Physics, China Academy of Engineering Physics, Mianyang, Sichuan 621999, China*
[4]*School of Future Technology, University of Chinese Academy of Sciences, Beijing 100049, China*

(Received 22 February 2024; accepted 11 June 2024; published 19 July 2024)

The emergence of shear bands is the universal cause of material failure in metallic glasses. In spite of relentless spirit, the structural origin, especially down to atomic level, of shear banding emergence is still an open question in disordered solids. Here, careful atomic simulations are carried out in $Cu_{50}Zr_{50}$ metallic glasses with various cooling histories. The icosahedral network formed by connected icosahedral clusters is recognized as the structural link between the glass formation process and shear banding emergence. First of all, it is found that the dominant structural evolution of glass transition is the competition between newly activated icosahedral clusters and the connection of existing ones. The glassy state as well as dynamics is then characterized by the level of connectivity of icosahedral clusters. This is evidenced by the power-law relation between the connectivity level and the relaxation time. Such connected icosahedral network is further found as the structural origin of the emergent inhomogeneous deformation field as well as the ultimate shear banding emergence upon loading. The emergence of shear bands is thus demonstrated as the collapse of the icosahedral network, which can be characterized as a "core-shell" structure in terms of our previously developed two-term gradient model. It is carefully demonstrated that atoms in the shell participate in dilatation and shear events while atoms in the inner core mainly undertake rotation motion. Our findings elaborate detailed physical images by tracing back to the critical glass transition process which provides a perspective in understanding the shear banding emergence.

DOI: 10.1103/PhysRevMaterials.8.073603

I. INTRODUCTION

The emergence of shear bands, characterized by high strain localization within a narrow band, is the main deformation mode in metallic glasses [1–3]. As the premise of crack initiation, the formation and fast evolution of shear bands act as the bottleneck that restricts the extensive applications of metallic glasses as the structural materials [4–11]. The paradigm that "structure controls properties" is generally accepted and has reached great success in crystalline solids [12,13] in which plasticity takes place via the motion of well-defined structural defects, such as dislocation and twinning. However, when it comes to metallic glasses, there is no common identification of structural defects that can be used to build the one-to-one relation with atomic-scale deformation field. This leads to the structural origin of transition from homogeneous deformation to unstable plastic flow localized in nanoscale shear bands, being still an enigma [14–20].

During decades of research, it has been validated that the inhomogeneity of deformation in metallic glasses is dependent on the cooling history [21–24]. For example, the emergence of a shear band can be more easily observed in glasses with a slower quenching process [25,26]. In this sense, it is reasonable to speculate that the critical glass transition of the cooling process determines the obtained glassy structure as well as the subsequent deformation field upon loading, i.e., the emergence of shear bands. Actually, such speculation has been partially validated by our recent simulated work which uncovers a large number of robust commonalities between shear banding and the glass transition [27]. Therefore, we are motivated that tracking the structural evolution of glass transition may open a path towards better understanding the structural origin of shear banding emergence.

The structural evolution of glass transition has aroused great interest since it is the key to forming an inherent disordered arrangement in metallic glass. First of all, many efforts have been made to use short-range order (SRO) to characterize the crucial dynamical arrest in glass-forming liquids [28–32]. Furthermore, compelling evidence has been given in both experiments [33–35] and simulations [36,37] that these short-range order clusters are prone to connect with each other during glass transition. This indicates that the connected short-range order clusters, i.e., medium-range order, may play an important role in the glass transition process [38–40]. Among them, icosahedral clusters with perfect fivefold symmetry appear to make the most contribution against crystallization, especially in the Cu-Zr system [41–43]. These icosahedral clusters exhibit strong spatial correlation and are prone to interpenetrate to form a stable structural network [44–46] with the static length scale only limited by the

*These authors contributed equally to this work.
†Contact author: lhdai@lnm.imech.ac.cn

simulation box [47]. The quantified relation between the connectivity of such network and its dynamic behavior [43,48,49], to some extent, reveals the correlation with glass transition. In addition, physical images about the partial collapse of the icosahedral network during plastic flow have also been uncovered [50–52]. This structural backbone has become a substantial unit for understanding the properties of metallic glass from the structural information in medium range [53–55].

In this work, we carry out a series of molecular dynamics simulations to prepare $Cu_{50}Zr_{50}$ glasses with different cooling rates which are then sheared. We follow the natural physical process from quenching to deformation, instead of purely researching glass transition or shear banding emergence. Our work reveals that the icosahedral network is the crucial structure that plays the dominant role on both the glass transition and the shear banding emergence. During the quenching process, four stages of the structural evolution are characterized. At stage 1 and stage 2, the birth of icosahedral clusters is the dominant structural evolution. At these two stages, the growing rate of icosahedral clusters increases with the drop of temperature. The leading behavior then turns to the connection of icosahedral clusters at the beginning of stage 3. In this stage, the existing isolated icosahedral clusters gather into small clusters constructed by hundreds of atoms. In stage 4, most of these clusters connect to each other and form a network going through the configuration. Such critical stage 3, which dominates the connection of icosahedral clusters, can be characterized as the beginning of structural differences of initial glass samples with various cooling histories. In the subsequent loading procedure, the evolution of the icosahedral network perfectly correlates with the emergence of shear bands. Here, with the help of a two-term gradient (TTG) model which is capable of decoupling the entangled shear-dilatation-rotation motion in disordered solids [56], we find the core-shell structure which controls the percolation of shear transformation zones [57,58]. Here, the atoms located in the shell mainly participate in dilatation and shear events while the atoms in the core are prone to do rotation motion. On this basis, we uncover a series of comprehensive physical images hidden behind the emergence of shear bands. By tracing back to the glass transition process, our work sheds light on understanding the structural origin of heterogeneous deformation in metallic glasses.

II. SIMULATION DETAILS

The molecular dynamics simulations were performed by the open source LAMMPS code [59]. The embedded-atom method (EAM) potential developed by Mendelev *et al.* [60] is adopted to describe the atomic interactions for the $Cu_{50}Zr_{50}$ metallic glass. The EAM model postulates that atoms are embedded within an electronic cloud that is mainly derived from the contributions of neighboring atoms. This model excels in depicting systems characterized by robust interatomic interactions, like alloys. The initial crystalline structure with the fcc phase was melted from 100 to 2100 K. After sufficient equilibration for 1 ns at 2100 K, the system was then quenched to a glass state at 100 K with cooling rates varying among 0.01, 0.1, 1, and 10 K/ps. Each of the obtained glass samples contained 55296 atoms with dimensions of $10 \times 10 \times 10\ \mathrm{nm}^3$ in the x, y, and z directions. The code employed several approximations for numerical calculations: (1) It simulated infinite atoms by using periodic boundary conditions in all dimensions to handle finite atoms. (2) In simulations, the rotational inertia, rotational energy, and charge of atoms were omitted. Thus, atoms were treated as points with mass. (3) The initial velocity was determined by temperature, mirroring the conditions in experimental settings. Simple shear loading, with a constant shear strain rate of $10^9\ \mathrm{s}^{-1}$, was adopted on the obtained glass samples at a low temperature of 100 K. Simulation boxes were changed to all triclinic to enable the occurrence of shear offset. The pressure and temperature were controlled using isothermal-isobaric ensembles [61] and a Nosé-Hoover thermostat [62,63] for the preparation and shearing process. The time step of the molecular dynamics was 0.002 ps.

III. RESULTS AND DISCUSSION

It is generally accepted that full icosahedral clusters are the typical short-range order clusters in Cu-Zr metallic glasses [25,41–43,64]. Using the Voronoi method, the local atomic packing could be characterized via the Voronoi polyhedron, which is a closed polyhedron enclosed by the mid-vertical planes of the lines connecting neighboring atoms. Classification of this polyhedron is denoted by the Voronoi index $\langle n_3, n_4, n_5, n_6, \ldots, n_i, \ldots\rangle$, where n_i denotes the number of i-edge polygons in the face of the polyhedron. Icosahedral clusters show perfect fivefold symmetry, and can be determined by Voronoi index $\langle 0,0,12,0\rangle$. It consists of a central atom and 12 surrounding atoms, forming a polyhedron with 20 triangular faces. Figure 1(a) shows an example of the connection of icosahedral clusters. Here, two icosahedral clusters are determined as "connected" if they share atoms. As shown in Fig. 1, most of icosahedral clusters are prone to connect together and thus constitute a structural network throughout the model $Cu_{50}Zr_{50}$ glass. This indicates that it is possible to discuss longer-range order in metallic glasses by concentrating on the behavior of interpenetrating icosahedral clusters, especially the biggest one that spans over the whole glass. In order to follow their evolving behavior quantitively, a structural parameter $S_{\max}$ is introduced as follows:

$$S_{\max} = \frac{n_{\mathrm{net}}}{n_{\mathrm{all}}}, \tag{1}$$

where n_{net} is the number of containing atoms in the biggest icosahedral network and n_{all} is the number of atoms in the whole system. In the glass system, icosahedral clusters can be connected or separately distributed. The connectivity of icosahedral clusters in this work is defined as the ratio of the content of the biggest connected icosahedral network to all of the icosahedral clusters. This can be quantified by the dimensionless ratio $S_{\max}/S_{\mathrm{FI}}$, where S_{FI} denotes the ratio of number of atoms in all of the icosahedral clusters to the number of atoms in the whole system.

Firstly, we analyze the sample with a cooling rate of 0.01 K/ps. The glass transition temperature can be identified by figuring out the turning point from the two-stage linear fit of the enthalpy-temperature plot, as shown in Fig. 1(b). To

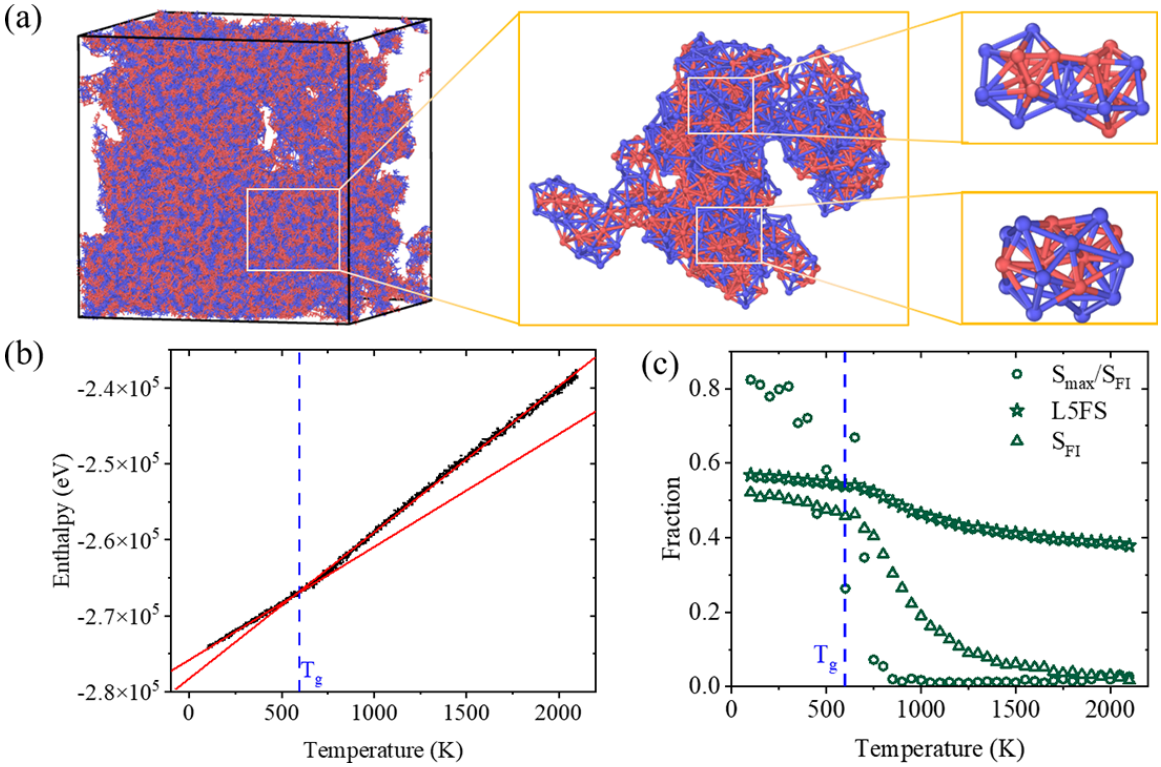

FIG. 1. (a) Snapshots show how icosahedral clusters connect each other (sharing atoms) to generate a big network. Neighboring atoms, within cutoff radius 3.8 Å, are connected by bonds. Atoms colored in red and blue represent Cu and Zr, respectively. (b) The evolution of enthalpy during the cooling history. The dashed line is used to point out the glass transition temperature. (c) The evolution of structural indicators as a function of temperature. The structural indicators contain S_{max}/S_{FI} (connectivity of the biggest icosahedral cluster), S_{FI} (fraction of full icosahedral clusters), and L5FS (local fivefold symmetry).

uncover the critical role of S_{max}/S_{FI} on the imperative glass transition process, we plot the evolution of S_{max}/S_{FI} during the quenching procedure, as shown in Fig. 1(c). It is clearly observed that S_{max}/S_{FI} grows significantly when the temperature is approaching the glass transition temperature. This gives brief evidence that the connection of icosahedral clusters is the potential structural origin hidden in the glass transition phenomena. For comparison, Fig. 1(c) also shows the evolution of the fraction of icosahedral clusters (S_{FI}) and the local fivefold symmetry (L5FS), both of which are protypical static structural indicators. All of the parameters are evolving during the quenching process, with S_{max}/S_{FI} being the most prominent, while S_{FI} and L5FS show limited variations in the glass transition regime. This gives direct evidence that S_{max}/S_{FI} is a better structural indicator on sketching the glass transition progress.

As shown in Fig 1(c), the turning point of the S_{FI}-temperature curve where S_{FI} begins to grow sharply takes place earlier than that of the S_{max}/S_{FI}-temperature curve. This difference suggests that S_{FI}, characterizing the birth or annihilation of short-range atomic packings, and S_{max}/S_{FI}, representing the longer-range process with the connection of existing icosahedral clusters, may operate at distinct stages during quenching. To further elucidate the progression of the formation of the icosahedral network, Fig. 2(a) presents a quantitative correlation between S_{max} and S_{FI}. An obvious change of the slope can be observed, with the turning point occurring close to the glass transition, as marked by the blue dashed line. It is noted that S_{FI} and S_{max} are quantitative reflections of the birth and connection of icosahedral clusters, respectively. Therefore, a competition between these two processes is expected. During the quenching process, firstly, the newborn of the icosahedral clusters plays the leading role as evidenced by the more pronounced increase of S_{FI} than that of S_{max} at temperatures over the glass transition temperature. After the turning point, the dominant mode changes to the connection of existing icosahedral clusters, with S_{max} growing with a faster rate than S_{FI}.

The details of such intriguing emergence of icosahedral network are further demonstrated by the evolution of S_{max}/S_{FI}, S_{FI} and $Q_{cluster}$, as shown in Fig. 2(b). Here, $Q_{cluster}$ is defined as the number of isolated icosahedral clusters which do not share atoms with other icosahedral clusters. On the one hand, the formation of newly isolated icosahedral clusters will lead to the increase of $Q_{cluster}$. On the other hand, the connection of existing icosahedral clusters is expected to drive the decrease of $Q_{cluster}$. In this sense, the evolution of $Q_{cluster}$ is capable of quantifying the competition between the birth and connection of icosahedral clusters. The growth or decay of $Q_{cluster}$ then demonstrates that the formation of newly isolated icosahedral clusters or their connection is the dominated mode. As shown in Fig. 2(b), the structural evolution of the glass transition process can be divided into four stages. Representative snapshots relating to each step are shown in Fig. 2(c). In stage 1, there is a gradual emergence of isolated icosahedral clusters whose fraction is growing slowly. In stage 2, an abrupt enhancement

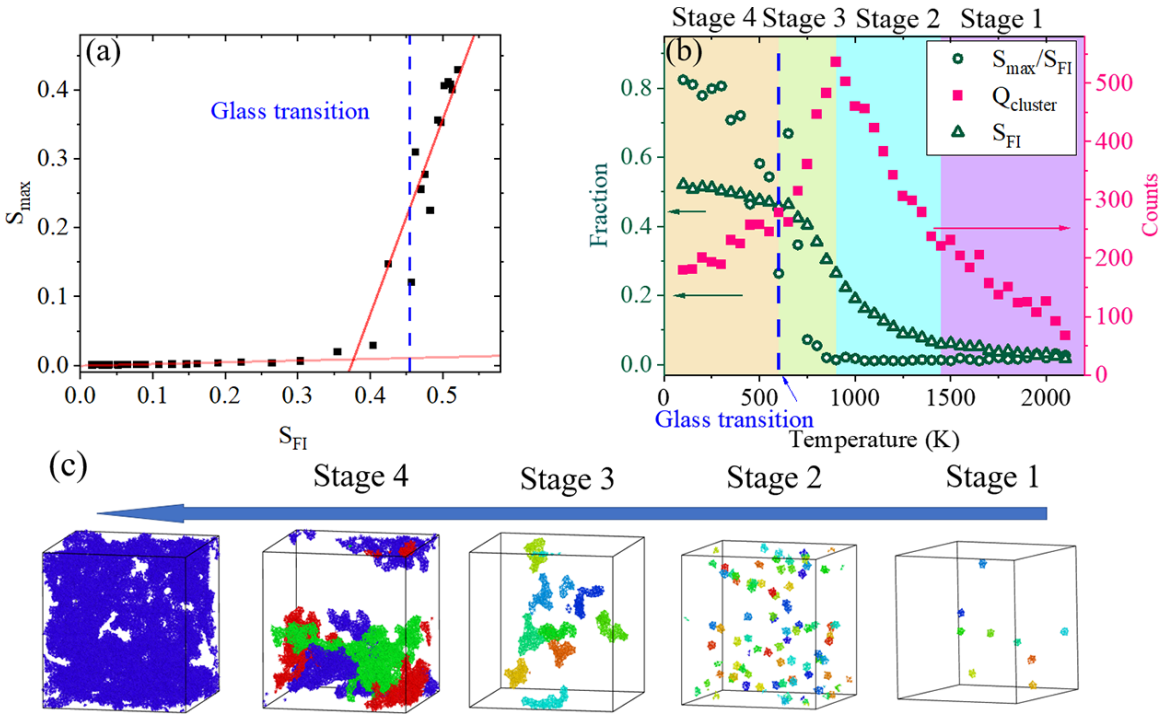

FIG. 2. (a) S_{max} as a function of S_{FI}. (b) The evolution of S_{max}/S_{FI}, S_{FI}, and $Q_{cluster}$ as a function of temperature. (c) Four stages of the cooling process, showing the initial distribution of icosahedral clusters (stage 1), the generation of new icosahedral clusters (stage 2), the connection of neighboring icosahedral clusters (stage 3), and the coalescence of connected clusters to form a structural network in the whole system (stage 4).

on the birth of icosahedral clusters accompanied by the growth of $Q_{cluster}$ implies that isolated icosahedral clusters begin to connect with neighboring ones to form the small connecting clusters. During the first two stages, the newborn event is the dominated mode, thus S_{max}/S_{FI} grows slowly. At the beginning of stage 3, it is seen that $Q_{cluster}$ begins to decrease while the value of S_{max}/S_{FI} grows significantly. This indicates that the dominant event turns to the connection of existing icosahedral clusters formed in previous stages, resulting in several larger networks, each containing hundreds of atoms. This shift overlaps with the turning point in Fig. 2(a). At the last stage, most of the icosahedral clusters link together to form a structural network that spreads over the whole system.

It is generally accepted that the cooling history controls the glass transition process as well as the obtained glassy structures. To clarify the critical role of each stage on the glass transition process, we carried out four cooling procedures with cooling rates of 0.01, 0.1, 1, and 10 K/ps, respectively. Figures 3(a)–3(c) show the exact evolution of S_{max}/S_{FI}, S_{FI}, and $Q_{cluster}$. The structural evolution of the samples exhibits a similar trend which is in line with the four stages shown in Fig. 2. Differences can be observed in terms of the amplitudes of structural indicators. For instance, samples that undergo slower cooling rates are prone to display higher levels for both S_{max}/S_{FI} and S_{FI}. This is in line with the existing literature that slow cooling rates are expected to lead to glasses with more ordered clusters [25,65].

Surprisingly, it is intriguing to observe that difference on structural evolution can only be captured after the beginning of stage 3. In stage 1 and stage 2, the structural evolutions for various cooling rates are perfectly overlapping with each other. This result is consistent for all three parameters, S_{max}/S_{FI}, S_{FI}, and $Q_{cluster}$. Referring to the significant observation that stage 3 is just right before the critical glass transition, it is reasonable to demonstrate that stage 3 plays the key role on the glass transition process. This is validated by further conducting cooling simulations with additional cooling procedures. Here, constant cooling rates of 0.1 and 10 K/ps for all stages is characterized as model 1 and model 3, respectively. In contrast, the strategy of model 2 is that a cooling rate of 0.1 K/ps is used in stage 3 while 10 K/ps is used in other stages. Figures 3(d)–3(f) show the corresponding structural evolutions. Intuitively, the structural evolutions of both model 1 and model 2 are almost identical to each other. This suggests that stage 3 controls the obtained glassy structure and is thus paramount during the glass transition process. In the structural scenario, the cooling history does not have an effect on the initial birth of the icosahedral clusters in the first two stages. However, sluggish quenching in stage 3 offers sufficient time for the connection of icosahedral clusters, thus leading to the various structures of the obtained glasses. Therefore, it can be concluded that stage 3, in which existing short-range icosahedral clusters connect to each other to form stiff structures with longer range, contributes most to the glass transition process. This is likely the underlying structural origin of the glass transition.

Having elaborated the critical role of the icosahedral network on glass transition, we next quantitatively discuss its correlation to the relaxation time, which is one of the critical dynamic signatures of the glass transition [66,67]. Firstly,

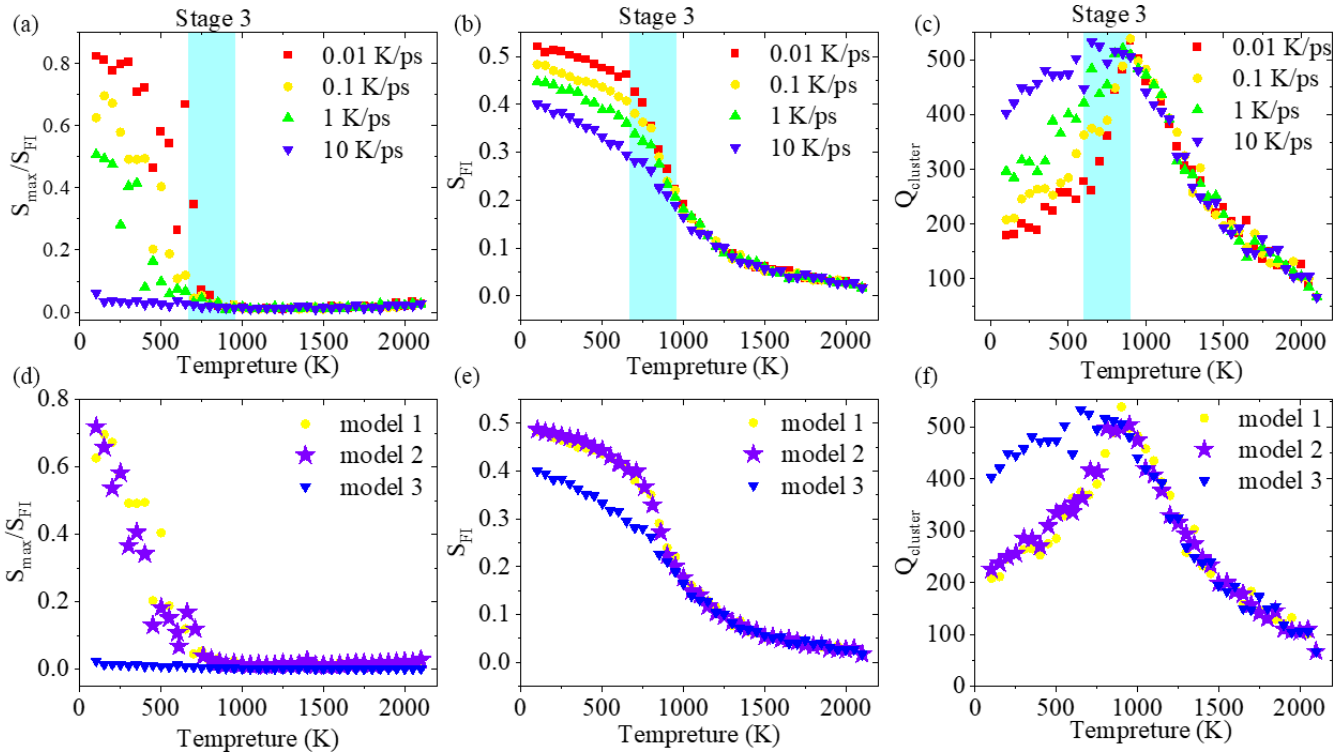

FIG. 3. (a)–(c) The evolution of S_{max}/S_{FI}, S_{FI}, and $Q_{cluster}$, respectively, during the cooling procedure with various cooling rates. (d)–(f) The evolution of S_{max}/S_{FI}, S_{FI}, and $Q_{cluster}$, respectively, during the cooling procedure with various cooling strategies. Model 1: constant cooling rate of 0.1 K/ps. Model 2: 0.1 K/ps in stage 3 while 10 K/ps for other stages. Model 3: constant cooling rate of 10 K/ps.

the self-intermediate scattering function (SISF) [68,69] is calculated:

$$F_s(q,t) = \frac{1}{N}\left\langle \sum_{j=1}^{N} \exp[i\vec{q}\cdot(\vec{r}_j(t) - \vec{r}_j(0))] \right\rangle. \quad (2)$$

Here, N is the total number of atoms and $\vec{r}_j(t) - \vec{r}_j(0)$ represents the displacement of atom j going through time t. $\vec{q}$ is the wave vector. Here, $|\vec{q}| = 2.7\,\text{Å}^{-1}$ corresponding to the first peak position of the structural factor. Then the α-relaxation time τ_α is obtained as the timescale when the SISF decays to $\exp(-1)$.

Figures 4(a)–4(d) show the SISF of supercooled liquids with various cooling rates. With decreasing temperature, it takes a longer time for atoms to lose memory about their initial occupying positions. It is intuitively seen that samples experiencing diverse cooling histories exhibit distinct dynamics properties. The conclusions acquired above reveal that the connectivity of icosahedral clusters grows with cooling, and the evolution of this indicator is various in four samples. In this sense, this is the fundamental evidence that icosahedral clusters play an important role in the relaxation dynamics process.

To obtain a more detailed relationship between S_{max} and τ_α, we plot τ_α as a function of S_{max} in Fig. 4(e). It exhibits a power law between τ_α and S_{max}. Factor S_0 is introduced to normalize S_{max}. Similarly, τ_α could be normalized by τ_0. As a result, we obtain the following power law between the structural indicator S_{max} and the relaxation time τ_α:

$$\tau_\alpha = \tau_0\left(\frac{S_{max}}{S_0}\right)^A, \quad (3)$$

where A is the exponent of the power law. Figure 4(e) clearly illustrates that the correlation between S_{max} and τ_α is well fitted by Eq. (3). Here, parameter A is shown geometrically as the slope of the fitted line. Obviously, parameter A exhibits different values for different cooling rates. Therefore, it is a factor between the icosahedral cluster and the α-relaxation time, which varies with samples produced in diverse process. The values of A are approximately 2.7, 4.2, 5.4, and 14.4 corresponding to the samples with cooling rates of 0.01, 0.1, 1 and 10 K/ps, respectively. As shown in Fig. 4, fitted lines have a potential to be vertical with the growth of cooling rates. In terms of Eq. (3), factor A is capable of measuring the susceptibility of dynamics to the connectivity of icosahedral clusters quantified by S_{max}. It is worth noting that the normalization coefficients S_0 and τ_0 for these four samples are equal within the margin of error, presenting as fitted lines intersecting at (S_0, τ_0) in geometry. Actually, they correspond to the structural parameter and relaxation time around 900 K, which is the beginning of stage 3.

It has been verified that the relationship between fivefold symmetry and τ_α can be fitted by an exponential function in various metallic glass systems [29]. However, as a parameter describing the extension of icosahedral clusters, S_{max} reflects both SROs and the spatial correlations among SROs that are beyond the nearest neighbors. Thus, the power-law

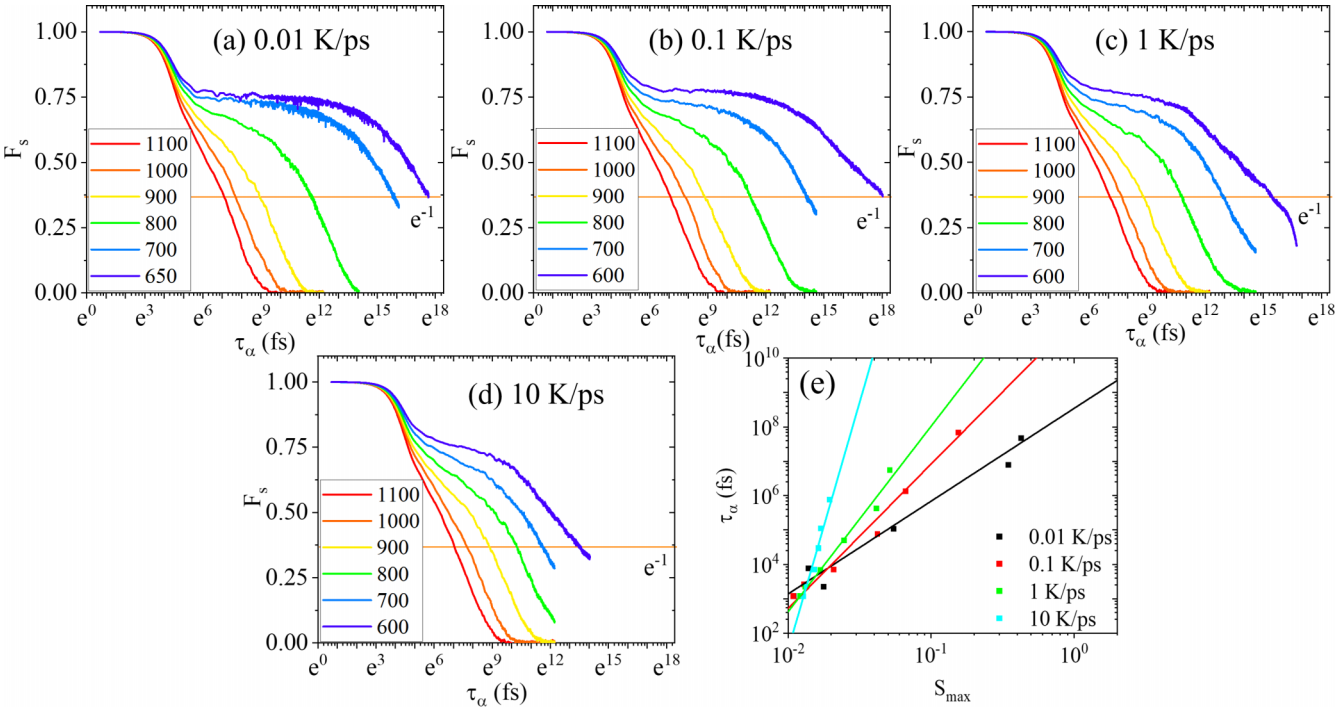

FIG. 4. Self-intermediate scattering functions for supercooled liquids in 1100, 1000, 900, 800, 700, and 600 K, respectively, among various cooling rates (a)–(d). The α-relaxation time is defined as the time when SIFI drops to $\exp(-1)$. The value of $\exp(-1)$ is denoted by the horizontal orange line. (e) The evolution of τ_α as a function of $S_{\max}$ which obeys the power law.

relation represents the interrelation between connected SROs and glassy dynamics.

We have elaborated that various cooling histories indeed bring different extents of connectivity in icosahedral networks which would induce diverse stability of the quenched glasses. This is properly the hidden structural origin of the cooling-history dependence of deformation responses in metallic glasses [25]. For example, glass samples with slower quenching rates have a higher level of icosahedral network and are thus more susceptible to shear banding. Thus, it is reasonable to speculate that the medium-range packing connection, acting as the icosahedral network, is the structural cause of strain localization and the subsequent shear banding emergence. In other words, the icosahedral network might be the critical clue going through both the quenching and the deformation process. This network provides a possibility for uncovering the mechanism hidden behind the cooling-rate-dependent deformation response which can be traced back to the glass transition. To validate this view, we carried out shear loading on the four glasses with different cooling rates.

Firstly, shear loading with a constant strain rate of $10^9\ \mathrm{s}^{-1}$ is applied to the obtained glass samples with various cooling rates. The stress-strain curves are given in Fig. 5(a). There is an initial linear increase of stress in the elastic deformation stage, until general strain $\varepsilon \sim 0.1$. Subsequently, the curve deviates from the linear growth and reaches the peak stress. After that, an abrupt decline of stress, namely stress overshoot, takes place, indicating the emergence of a shear band. Distinct peak stress and similar plastic flow stress indicate that the initial structures are strongly correlated with the peak stress, but evidently do not influence the flow stress. The snapshots in Fig. 5(b) directly present the evolution of the strain field, colored by atomic effective strain Λ, which covers both affine and nonaffine parts of displacement [70,71]. Obviously, samples with slower cooling rates show higher levels of susceptibility to strain localization. This is the intuitive evidence that an icosahedral network controls the inherent deformation localization in metallic glasses. Furthermore, we place an emphasis on discussion about the relation between the behavior of the icosahedral network and the emergence of shear bands. Here, we focus on the atoms occupying the single shear band shown in Fig. 5. Specifically, the largest connectivity of icosahedral clusters ($S_{\max}/S_{\mathrm{FI}}$) is then calculated based on these atoms. The parameter $S_{\max}/S_{\mathrm{FI}}$, which will be discussed later, is defined as the ratio between numbers of atoms constituting the icosahedral network and those constructing the icosahedral clusters in the region of the shear band.

Figure 6 shows the change of $S_{\max}/S_{\mathrm{FI}}$ in the single shear band. It is seen that $S_{\max}/S_{\mathrm{FI}}$ declines in the elastic regime in Fig. 5(a). Subsequently, a precipitous drop in $S_{\max}/S_{\mathrm{FI}}$ to almost zero is observed, indicating the spontaneous collapse of the icosahedral network during the emergence of shear bands. During the plastic flow regime, $S_{\max}/S_{\mathrm{FI}}$ stays at around 0 for all glass samples. This indicates the similar structure of glasses in plastic flow states. Referring back to Fig. 5(a), $S_{\max}/S_{\mathrm{FI}}$ is capable of reflecting the structural evolution which perfectly matches the overall stress-strain curves.

Obviously, there is a mutual influence between structure and deformation. On the one hand, the deformation field is controlled by the inhomogeneous structure induced by the spatial distribution of connected icosahedral clusters. On the other hand, such icosahedral network, in turn, can be broken once the emergence of a shear band takes place. This result is

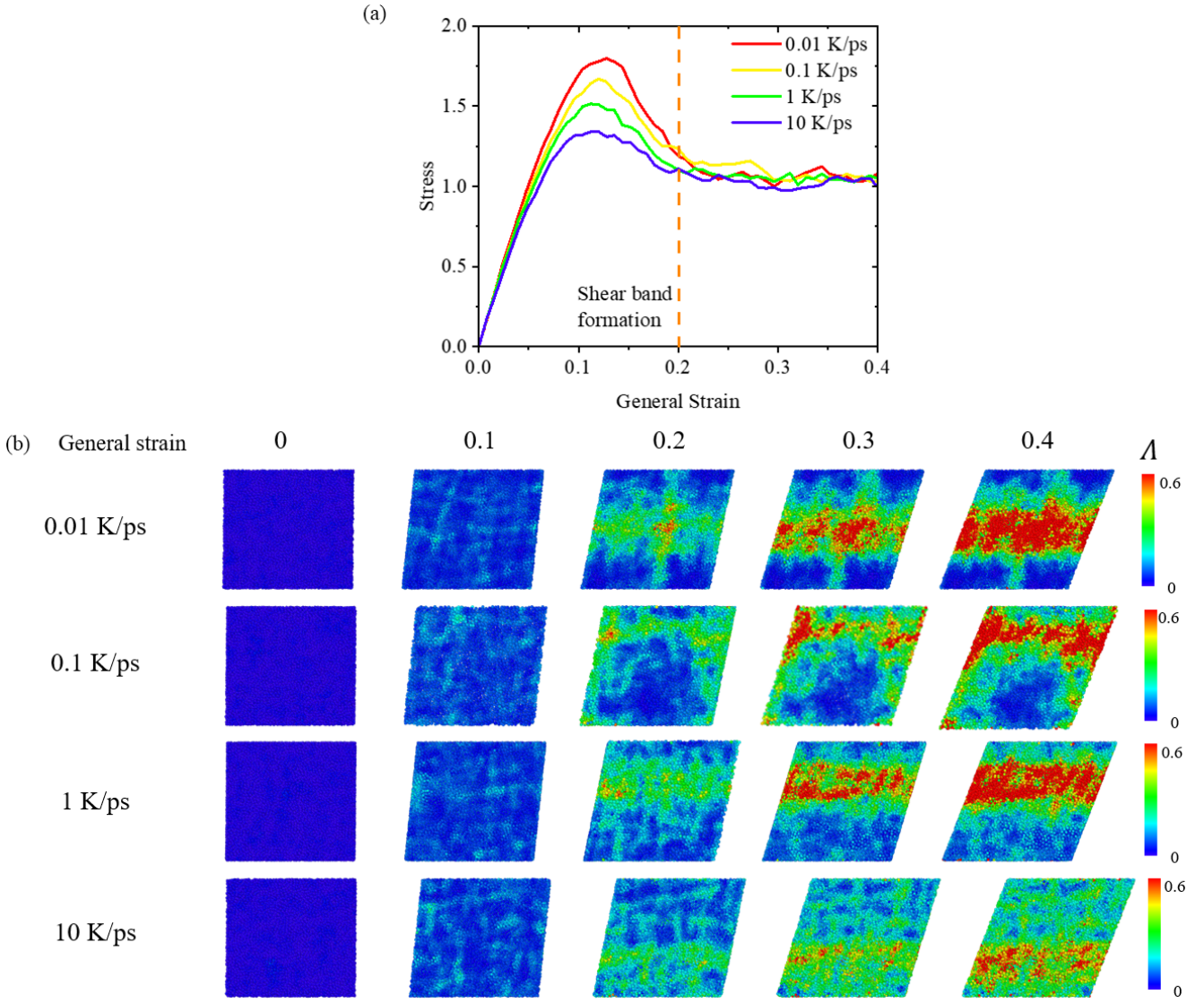

FIG. 5. (a) Simulated stress-strain curve under the simple shear loading. The dashed line indicates the formation of one shear band. (b) The snapshots show the localization process by monitoring atomic effective strain.

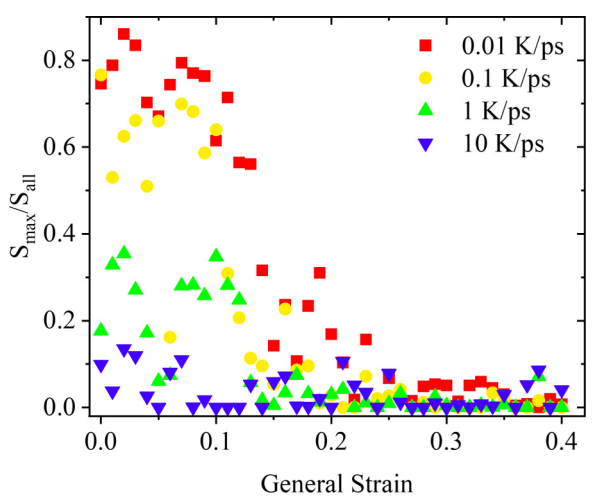

FIG. 6. The evolution of S_{max}/S_{FI} in shear bands for metallic glass prepared by various cooling rates.

consistent among all of the simulated samples. To investigate the specific influence between long-range packing and deformation localization, we will thoroughly analyze the sample quenching at a rate of 0.01 K/ps.

It is well known that full icosahedral clusters are a kind of hard short-range order structure. In this connection, it is predicted that the icosahedral network might be the obstacle of deformation. In order to explicitly demonstrate the deformation response of the icosahedral network, the normalized atomic strain in each icosahedral cluster as a function of cluster size is given in Fig. 7. Here, microscopic strain Λ for an icosahedral cluster is the mean value of atomic strain for atoms constructing the cluster and it is normalized by general strain ε. When Λ/ε equals 1, it represents the average strain for the overall sample. In contrast, the value far beyond or below 1 implies deformation localization or nearly no deformation, respectively. For comparison, various applied strains are considered. It clearly reveals that a large magnitude of microscopic strain is always located inside clusters with smaller

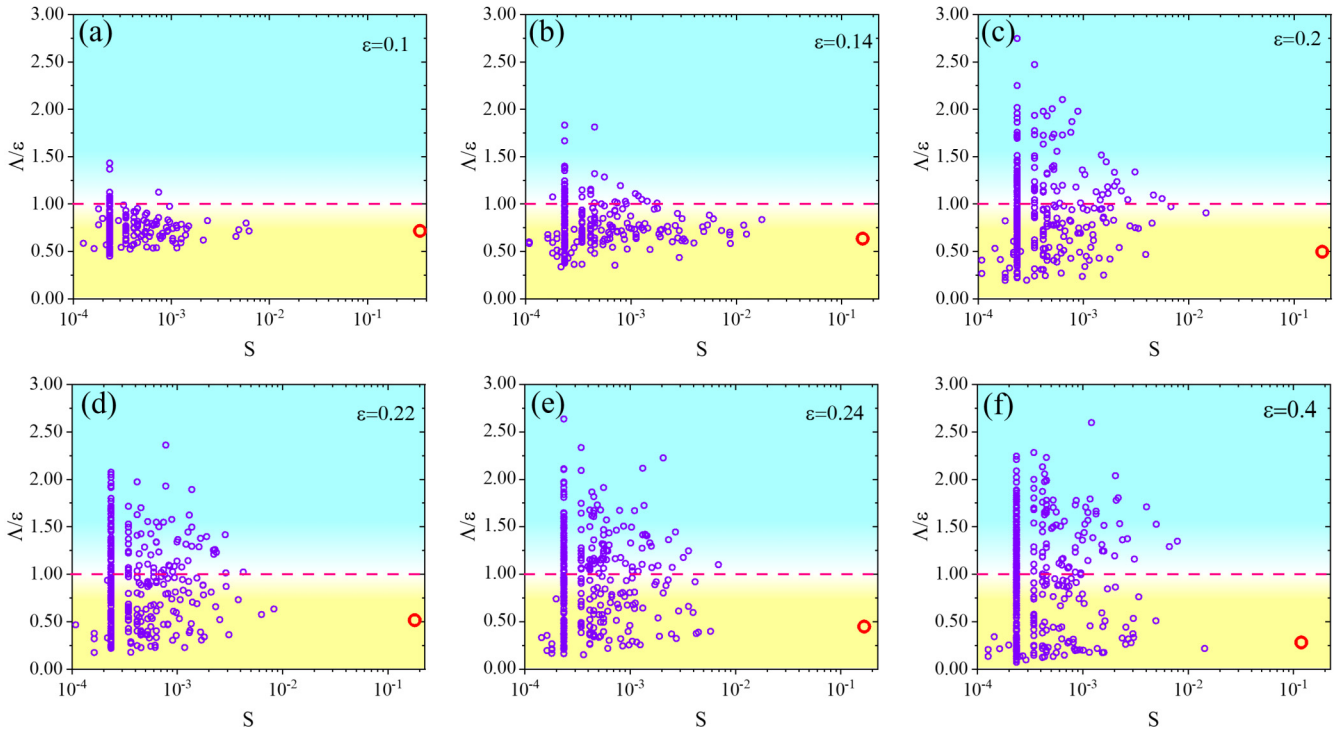

FIG. 7. The correlation between average magnitudes of microscopic strain Λ normalized by macroscopic strain ε and the size of icosahedral clusters S which means the quantity of atoms forming the cluster. The evolution in different deformation stages is shown in (a)–(f), including the early stage of deformation (a), the moment just before shear banding emergence (b), the stage of the emergence of a shear band (c)–(e), and the formation of a mature shear band (f). The biggest icosahedral network is specially marked by the red circle.

size, with the largest icosahedral cluster (marked by a red circle in Fig. 7) undergoing the relatively small deformation far below the average. This trend is more pronounced as the applied strain increases.

It is widely believed that shear transformation zones (STZs), manifesting as flow defects in metallic glasses, are originally activated in soft regions, where atomic clusters are unstable [18,64]. The icosahedral network that wraps these areas could be thought of as a barrier that limits the arbitrary propagation of these initially deformed regions. With growing general strain, regions of network neighboring STZs are activated and soften with atoms peeling from it. Finally, it leads to the percolation transition and shear banding formation. In this connection, our results are consistent with these reported works.

To discuss the correspondence between structural evolution and the deformation field, we introduce the TTG model developed in our previous work [56]. The model decouples atomic deformation covering affine and nonaffine parts to elementary atomic motion, that is, shear, dilatation, and rotation. Firstly, displacement gradient tensor H^i_{mn} and strain gradient η^i correspond to affine and nonaffine deformation, respectively. For the affine part, H^i_{mn} could be rearranged to three components, as $R^{H,i}_{mn} = \frac{1}{2}(H^i_{mn} - H^i_{nm})$, $S^{H,i}_{mn} = [\frac{1}{2}(H^i_{mn} - H^i_{nm}) - \frac{1}{3}(H^i_{ll} I_{mn})]$, and $D^{H,i}_{mn} = \frac{1}{3}(H^i_{ll} I_{mn})$, where I_{mn} is the identity tensor. Furthermore, following the decoupling method of Fleck and Hutchinson [72], strain gradient η^i can be decoupled into $S^{\eta,i}_{kmn} = \frac{1}{6}(\eta'^i_{kmn} + \eta'^i_{mnk} + \eta'^i_{nkm})$, $R^{\eta,i}_{kmn} = \eta'^i_{kmn} - S^{\eta,i}_{kmn}$, and $D^{\eta,i}_{kmn} = \frac{1}{8}(\eta^i_{mll}\delta_{kn} + \eta^i_{kll}\delta_{mn})$. Here, δ_{mn} is the Kronecker symbol. After decoupling of the deformation field, transformation factors ξ_R, ξ_S, and ξ_D for rotation, shear, and dilatation, respectively, could be defined as follows:

$$\xi^i_R = \sqrt{R^{H,i}_{mn} R^{H,i}_{mn}} \sqrt{R^{\eta,i}_{kmn} R^{\eta,i}_{kmn}},$$
$$\xi^i_S = \sqrt{S^{H,i}_{mn} S^{H,i}_{mn}} \sqrt{S^{\eta,i}_{kmn} S^{\eta,i}_{kmn}},$$
$$\xi^i_D = \sqrt{D^{H,i}_{mn} D^{H,i}_{mn}} \sqrt{D^{\eta,i}_{kmn} D^{\eta,i}_{kmn}}. \quad (4)$$

Based on the quantitative description of shear, dilation, and rotation for both affine and nonaffine deformation, the participation fraction is defined as

$$\chi^i_P = \frac{\frac{\xi^i_P}{\xi^M_P}}{\sqrt{\left(\frac{\xi^i_R}{\xi^M_R}\right)^2 + \left(\frac{\xi^i_D}{\xi^M_D}\right)^2 + \left(\frac{\xi^i_S}{\xi^M_S}\right)^2}}, \quad (5)$$

where the subscript P in ξ^i_P and ξ^M_P could be replaced by R, S, and D for rotation, shear, and dilatation, respectively. ξ^i_P/ξ^M_P is the ratio of transition factors and their mean values. The determination of the dominant event for an atom is based on comparing the participation fraction. The highest value of this fraction identifies the deformation region as either shear dominated (SDZs), dilation dominated (DDZs), or rotation dominated (RDZs). In this way, shear banding emergence can be demonstrated as the cooperative evolution of SDZs, DDZs, and RDZs.

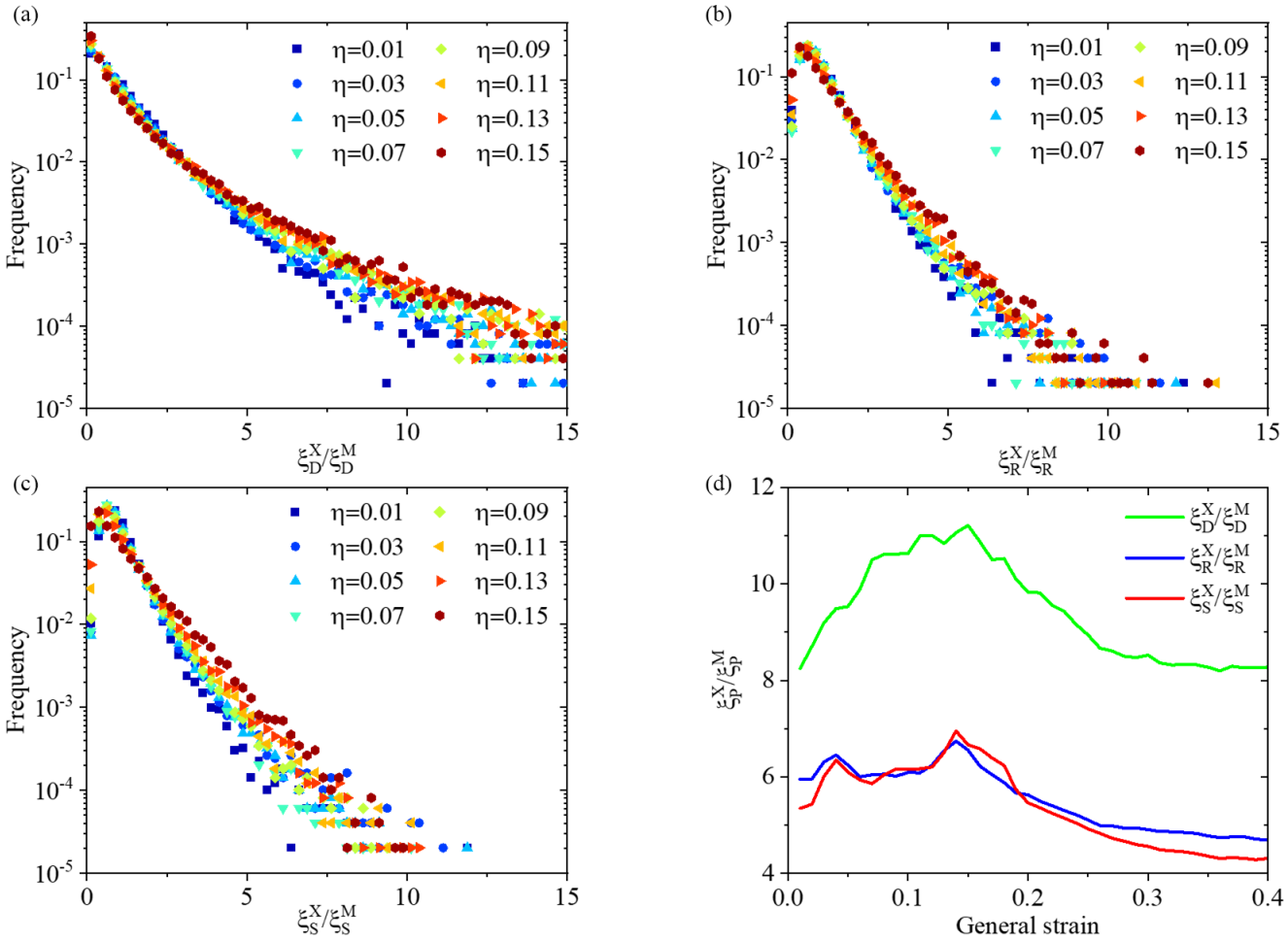

FIG. 8. The extreme analysis of rotation, dilatation, and shear events of atoms in the shear band. Statistical distribution of dilatation (a), rotation (b), and shear (c) transformation factors normalized by mean values at various general strains. (d) The evolution of extreme value with the growth of applied strain.

First, the extreme value theory [73] is applied to analyze the initial deformation localization. Figures 8(a)–8(c) show the probability density distribution of dimensionless ratios ξ_S^X/ξ_S^M, ξ_D^X/ξ_D^M, and ξ_R^X/ξ_R^M, which are atomic transition factors normalized by their mean values. Since these indicators are dimensionless, it is reasonable to compare the initial localization behavior of shear, dilatation, and rotation. It is intuitive that the maximum probability of factors always stays around 1 for all of the applied macroscopic strains. The statistical distribution of these factors is synchronously decreasing, except the long tail behavior. This difference implies inhomogeneous flow for events of shear, rotation, and dilatation.

Based on the extreme value theory, we then pick out and track atoms with the top 2% of transformation factors related to the shear, dilatation, and rotation events, respectively. Atoms corresponding to these extreme values are expected to be the origin of strain burst and deformation localization. These transformation actors ξ_P^X are then normalized by the mean values ξ_P^M of atoms residing in the whole configuration. Here, the subscript P in ξ_P^X and ξ_P^M can be replaced by D for dilatation, R for rotation, and S for shear, respectively. The ratio ξ_P^X/ξ_P^M is an indicator to measure irregularity for the obtained deformation events, that is, long-tailing behavior. The change of this indicator ξ_P^X/ξ_P^M as a function of applied strains is shown in Fig. 8(d). It is seen that the extreme values of the parameter for dilatation goes beyond that of shear and rotation. This result indicates that dilatation plays the dominant role in the initial stage of deformation. This is in line with our previous simulated work [56].

Next, we discuss the structural responses accompanying the evolution of SDZs, DDZs, and RDZs. We pick atoms representing shear dominant, dilatation dominant, and rotation dominant, respectively, and pay attention to the fraction of atoms constituting the biggest icosahedral clusters. The result is plotted in Fig. 9(a). The ratio of atoms belonging to the stiff network that exhibit rotation-dominant events is consistently larger than that of the shear-dominant and dilatation-dominant events. This indicates that RDZs are prone to overlap with the biggest icosahedral network. In contrast, DDZs and SDZs are more likely to be related to regions with relatively looser atomic packing. The consequence reinforces the idea that atomic motion in the hard region is apt to rotation.

As shown in Fig. 9(a), an abrupt drop in the fraction of atoms participating in these three events takes place when the sample strain exceeds 0.1, corresponding to the emergence of stress overshoot shown in Fig. 5(a). The phenomena indicates that a large extent of destruction for the icosahedral network begins after the sample strain exceeds 0.1. Therefore, we

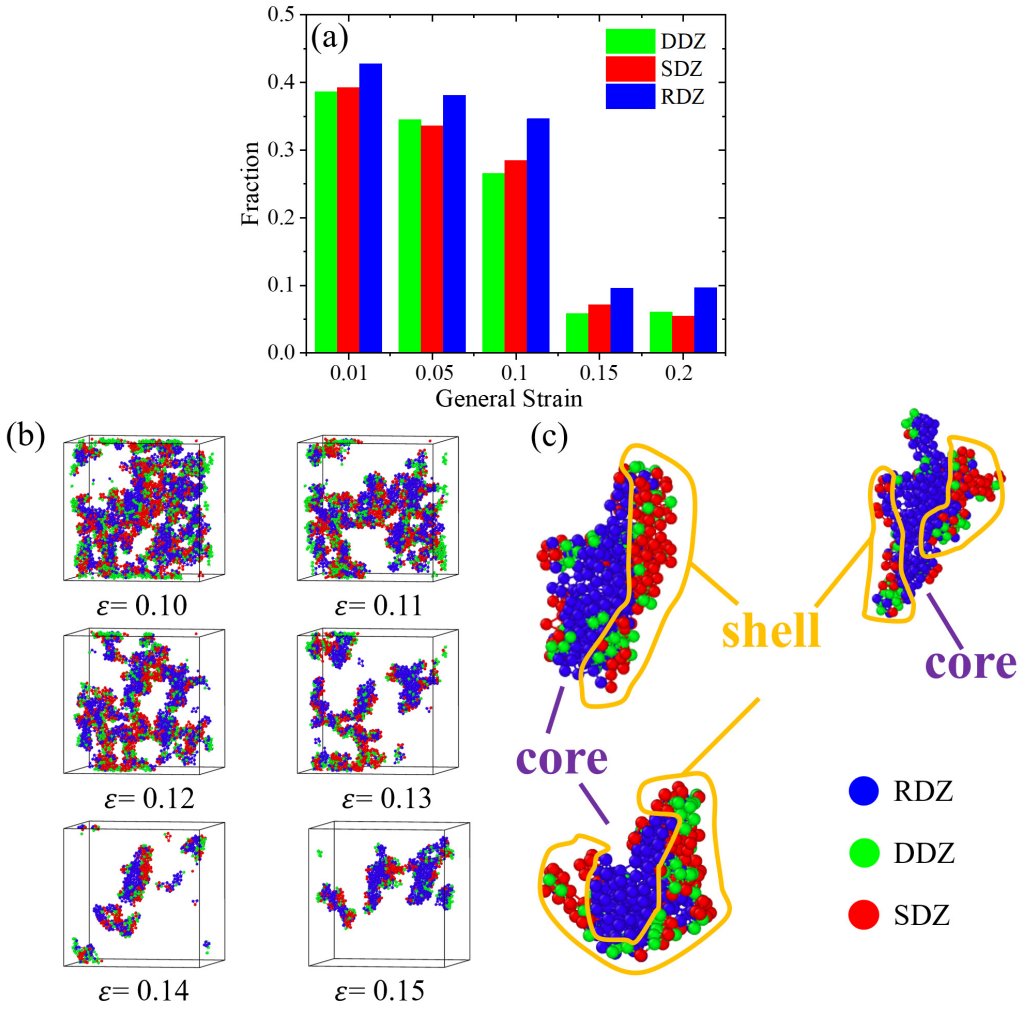

FIG. 9. (a) Ratio of atoms constructing the biggest cluster over atoms exhibiting shear dominant, dilatation dominant, and rotation dominant, respectively. (b) Spatial evolution of the biggest connected icosahedral network in the shear band. The snapshots are shown in the 20 Å slice of shear banding zones at different strain magnitudes. Atoms undergoing SDZs, DDZs, and RDZs are denoted by red, green, and blue, respectively. (c) Parts of the core-shell structure taken from the icosahedral network.

specifically analyze the atomic behaviors in the icosahedral network during this period. Figure 9(b) intuitively presents the spatial distribution of SDZs, DDZs, and RDZs, with the tumbling evolution for the icosahedral network in general strain from 0.1 to 0.15. Comparing the snapshots of samples prior to and after deformed stages, the vanished parts are usually atoms located at the edge of the network. These are typically SDZs and DDZs enfolding RDZs. This result inspires us to analyze the icosahedral network as a core-shell structure as sketched in Fig. 9(c). The atoms in outer shells neighboring soft and deformed regions mainly move via shear and dilatation, thus acting as the SDZs and DDZs. In contrast, the internal cores, being stable and stiff parts, display as RDZs. With applied strains, SDZ and DDZ shells, wrapping RDZ cores, peel from the icosahedral network, ultimately causing its collapse.

From these results, we demonstrate that structure has a great impact on deformation motion. The behavior of atoms located in the network follows the core-shell rule during the whole process of destruction of the network. The next task is to demonstrate, how the element motions drive the deconstruction of the biggest network. Subsequently, we will demonstrate that the atomic events, in turn, have the effect of destruction for the icosahedral network by analyzing atoms peeling from the icosahedral network.

For explicit comprehension, we define the atoms falling out from the network as the collection of atoms residing in the icosahedral network in the former moment in simulation while not belonging to the network in the next moment. Based on these explanations, Fig. 10(a) presents the fraction of dominant atomic motion presenting rotation, shear, and dilatation, respectively, when peeling from the network. Firstly, fractions of SDZs, DDZs, and RDZs overlap during the elastic deformation stage. Then, the fraction of RDZs sharply increases at the beginning of strain localization while DDZs and SDZs are still synchronized. After the general strain of 0.2, which is the moment when the network is exhaustively destroyed, the fraction for RDZs, DDZs, and SDZs begins to fluctuate in a disorderly manner, as shown in Fig. 10(a). This is due to the structural change that after the formation of shear bands, the biggest icosahedral network is broken.

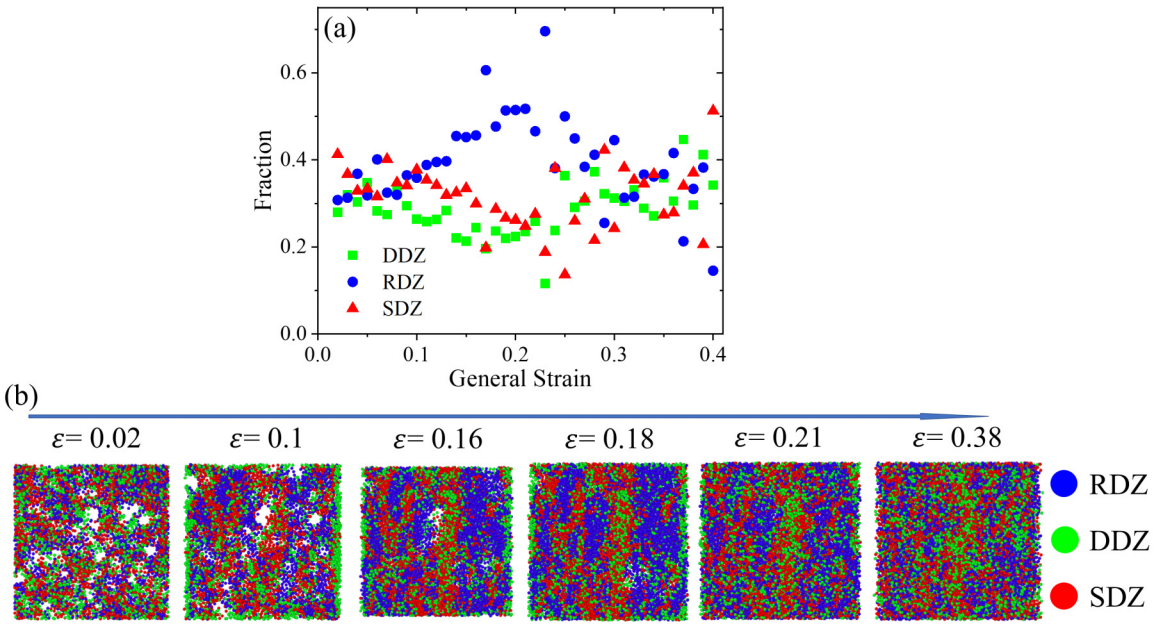

FIG. 10. (a) Fractional evolution of atoms exhibiting SDZs, DDZs, and RDZs peeling from the biggest cluster. (b) Spatial evolution of atoms presenting SDZs, DDZs, and RDZs beyond the biggest cluster with the growth of general strain.

To further illustrate the specific atomic motions that control the breakdown of the icosahedral network, Fig. 10(b) shows a series of snapshots of the part beyond the biggest icosahedral cluster. Actually, it shows the complement of Fig. 9(b). The holes in the snapshots are the areas that the network locates, which we call the "network rich area" while other parts correspond to the "network poor area." With applying strain, atoms peel from the biggest cluster and fill the blank in the snapshot. It is intuitive that atoms controlled by rotation shear and dilatation are scattered randomly during the initial deformation. After the general strain at 0.1, the fraction of RDZs grows remarkably. When the general strain reaches 0.18, there is an obvious sandwich structure of two rotation-dominant gathering regions separated by regions with mixed distribution of shear dominant and dilatation dominant. That implies that these bulk atomic clusters colored in blue fall off from the network corresponding to the sudden growth of RDZs in Fig. 10(a).

The physical image of atoms falling out from the network could be sketched based on the core-shell structure. Firstly, dilatation activates the initial deformation in soft regions, while the hard icosahedral network mainly undertakes rotation and acts as the obstacle hindering the development of activated STZs.

As applied strain increases, STZs confined in the network poor area excite the neighboring part of the icosahedral network, inducing softening of the outer shells of the icosahedral network. The outer shells, occupied by unstable SDZs and DDZs, firstly collapse, accompanied by the transformation of the inner cores from RDZs to SDZs or DDZs. Subsequently, these transition parts become outer shells and ultimately fall off from the network. This process sustains until the deformation localization begins at ∼0.1, which corresponds to the network collapsing rapidly. The collapse of such core-shell structure thus can be characterized as a positive feedback process with the continuing exposed shell being activated. This is the hidden structural process accompanying the shear banding emergence.

IV. CONCLUSION

Shear band as a consequence of the deformation-controlled glass transition, has a uniform structural origin with the temperature-controlled glass transition, that is, the topology of the medium-range ordered structure, i.e., the connection of icosahedral clusters. Instead of studying these two processes in isolation, we followed the natural preparation-deformation process and investigated the mechanism hidden behind samples with various cooling rates exhibiting a discrepant extent of inhomogeneous deformation. Furthermore, we demonstrated quantitatively that the icosahedral network also plays a crucial role in controlling dynamical heterogeneity. This is in line with our recent work that the topology instead of atomic ordering or flow defects density exhibits the dominant character [74]. Dating back to the formation of this vital network, stage 3 (ranging from 900 to 600 K) is the fateful period during the quenching process. According to atomic motion, the icosahedral network, acting as the structural origin of shear banding emergence, could be explained as a core-shell structure, which divides the network into an outer unstable shell occupied by SDZs or DDZs, and an inner stable core accommodating RDZs. The collapse of the icosahedral network, which accommodates plastic deformation, is actually the procedure in which atoms in the outer shell are activated, softened, and finally peeled from the network. Then, the newly exposed part turns into a shell, activated by shear and dilatation again. As the deformation goes on, there is an abrupt collapse of the icosahedral network, corresponding to the emergence of a shear band. This process is accompanied by the disruption of RDZs wrapped by SDZs and DDZs. The connected icosahedral clusters then act as a bridge to

link glass transition and shear banding emergence. These observations thus open up a path toward understanding the material softening mechanism and physical process of shear band emergence in amorphous solids by tracking back to the critical glass transition process.

ACKNOWLEDGMENTS

This work is supported by the NSFC Basic Science Center Program for "Multiscale Problems in Nonlinear Mechanics" (Grant No. 11988102), the Strategic Priority Research Program (Grants No. XDB22040302 and No. XDB22040303), and the Key Research Program of Frontier Sciences (Grant No. QYZDJSSWJSC011). This work is also supported by the Opening Project of State Key Laboratory of Explosion Science and Technology (Beijing Institute of Technology, Grant No. KFJJ23-03M) and Ye Qisun Science Foundation of National Natural Science Foundation of China (Grant No. U2141204). The numerical calculations in this study are carried out on the ORISE Supercomputer.

[1] A. L. Geer and E. Ma, Bulk metallic glasses: At the cutting edge of metals research, MRS Bull. **32**, 611 (2007).
[2] C. A. Schuh, T. C. Hufnagel, and U. Ramamurty, Mechanical behavior of amorphous alloys, Acta Mater. **55**, 4067 (2007).
[3] Y. Wu, H. Bei, Y. L. Wang, Z. P. Lu, E. P. George, and Y. F. Gao, Deformation-induced spatiotemporal fluctuation, evolution and localization of strain fields in a bulk metallic glass, Int. J. Plast. **71**, 136 (2015).
[4] F. Spaepen, A microscopic mechanism for steady state inhomogeneous flow in metallic glasses, Atca Metall. **25**, 407 (1977).
[5] A. L. Greer, Y. Q. Cheng, and E. Ma, Shear bands in metallic glasses, Mater. Sci. Eng., R **74**, 71 (2013).
[6] T. Egami, T. Iwashita, and W. Dmowski, Mechanical properties of metallic glasses, Metals (Basel, Switz.) **3**, 77 (2013).
[7] M. L. Manning, E. G. Daub, J. S. Langer, and J. M. Carlson, Rate-dependent shear bands in a shear-transformation-zone model of amorphous solids, Phys. Rev. E **79**, 016110 (2009).
[8] J. S. Langer, Microstructural shear localization in plastic deformation of amorphous solids, Phys. Rev. E **64**, 011504 (2001).
[9] B. A. Sun and W. H. Wang, The fracture of bulk metallic glasses, Prog. Mater Sci. **74**, 211 (2015).
[10] W. Li, H. Bei, and Y. Gao, Effects of geometric factors and shear band patterns on notch sensitivity in bulk metallic glasses, Intermetallics **79**, 12 (2016).
[11] M. Q. Jiang and L. H. Dai, On the origin of shear banding instability in metallic glasses, J. Mech. Phys. Solids **57**, 1267 (2009).
[12] Y. Fan, Y. N. Osetsky, S. Yip, and B. Yildiz, Onset mechanism of strain-rate-induced flow stress upturn, Phys. Rev. Lett. **109**, 135503 (2012).
[13] G. R. Odette, M. J. Alinger, and B. D. Wirth, Recent developments in irradiation-resistant steels, Annu. Rev. Mater. Res. **38**, 471 (2008).
[14] H. Tong and H. Tanaka, Revealing hidden structural order controlling both fast and slow glassy dynamics in supercooled liquids, Phys. Rev. X **8**, 011041 (2018).
[15] J. C. Ye, J. Lu, C. T. Liu, Q. Wang, and Y. Yang, Atomistic free-volume zones and inelastic deformation of metallic glasses, Nat. Mater. **9**, 619 (2010).
[16] Z. Fan, E. Ma, and M. L. Falk, Predicting the location of shear band initiation in a metallic glass, Phys. Rev. Mater. **6**, 065602 (2022).
[17] D. Richard *et al.*, Predicting plasticity in disordered solids from structural indicators, Phys. Rev. Mater. **4**, 113609 (2020).
[18] J. Ding, S. Patinet, M. L. Falk, Y. Cheng, and E. Ma, Soft spots and their structural signature in a metallic glass, Proc. Natl. Acad. Sci. USA **111**, 14052 (2014).
[19] T. Egami, W. Dmowski, and C. W. Ryu, Medium-range order resists deformation in metallic liquids and glasses, Metals (Basel, Switz.) **13**, 442 (2023).
[20] X. Wei, B. Xu, and P. Guan, A link between mechanical heterogeneity and nontrivial local structural power-law response in a model metallic glass, J. Non.-Cryst. Solids **578**, 121345 (2022).
[21] Z. Y. Yang and L. H. Dai, Giant configurational softening controls atomic-level process of shear banding in metallic glasses, Phys. Rev. Mater. **5**, 123602 (2021).
[22] Z. Zhang, J. Ding, and E. Ma, Shear transformations in metallic glasses without excessive and predefinable defects, Proc. Natl. Acad. Sci. USA **119**, e2213941119 (2022).
[23] J. Ding, L. Li, N. Wang, L. Tian, M. Asta, R. O. Ritchie, and T. Egami, Universal nature of the saddle states of structural excitations in metallic glasses, Mater. Today Phys. **17**, 100359 (2021).
[24] B. Shang, W. Wang, A. L. Greer, and P. Guan, Atomistic modelling of thermal-cycling rejuvenation in metallic glasses, Acta Mater. **213**, 116952 (2021).
[25] Y. Q. Cheng, A. J. Cao, H. W. Sheng, and E. Ma, Local order influences initiation of plastic flow in metallic glass: Effects of alloy composition and sample cooling history, Acta Mater. **56**, 5263 (2008).
[26] Z. Y. Yang, Y. J. Wang, and L. H. Dai, Susceptibility of shear banding to chemical short-range order in metallic glasses, Scr. Mater. **162**, 141 (2019).
[27] Z. Y. Yang and L. H. Dai, Towards commonality between shear banding and glass-liquid transition in metallic glasses, Phys. Rev. Mater. **6**, L100602 (2022).
[28] F. Spaepen, Five-fold symmetry in liquids, Nature (London) **408**, 781 (2000).
[29] Y. C. Hu, F. X. Li, M. Z. Li, H. Y. Bai, and W. H. Wang, Five-fold symmetry as indicator of dynamic arrest in metallic glass-forming liquids, Nat. Commun. **6**, 8310 (2015).
[30] J. P. K. Doye and D. J. Wales, The structure and stability of atomic liquids: From clusters to bulk, Science **271**, 484 (1996).
[31] D. R. Nelson, Polytetrahedral order in condensed matter, Solid State Phys. **42**, 1 (1989).
[32] S. W. Lee, M. Y. Huh, E. Fleury, and J. C. Lee, Crystallization-induced plasticity of Cu-Zr containing bulk amorphous alloys, Acta Mater. **54**, 349 (2006).
[33] A. Hirata, P. Guan, T. Fujita, Y. Hirotsu, A. Inoue, A. R. Yavari, T. Sakurai, and M. Chen, Direct observation of local atomic order in a metallic glass, Nat. Mater. **10**, 28 (2011).

[34] S. Hilke, H. Rösner, D. Geissler, A. Gebert, M. Peterlechner, and G. Wilde, The influence of deformation on the medium-range order of a Zr-based bulk metallic glass characterized by variable resolution fluctuation electron microscopy, Acta Mater. **171**, 275 (2019).

[35] D. B. Miracle, A structural model for metallic glasses, Nat. Mater. **3**, 697 (2004).

[36] P. Zhao, J. Li, J. Hwang, and Y. Wang, Influence of nanoscale structural heterogeneity on shear banding in metallic glasses, Acta Mater. **134**, 104 (2017).

[37] H. W. Sheng, W. K. Luo, F. M. Alamgir, J. M. Bai, and E. Ma, Atomic packing and short-to-medium-range order in metallic glasses, Nature (London) **439**, 419 (2006).

[38] D. Ma, A. D. Stoica, and X. L. Wang, Power-law scaling and fractal nature of medium-range order in metallic glasses, Nat. Mater. **8**, 30 (2009).

[39] T. Fujita, K. Konno, W. Zhang, V. Kumar, M. Matsuura, A. Inoue, T. Sakurai, and M. W. Chen, Atomic-scale heterogeneity of a multicomponent bulk metallic glass with excellent glass forming ability, Phys. Rev. Lett. **103**, 075502 (2009).

[40] C. W. Ryu and T. Egami, Medium-range atomic correlation in simple liquids. I. Distinction from short-range order, Phys. Rev. E **104**, 064109 (2021).

[41] Y. Q. Cheng, E. Ma, and H. W. Sheng, Alloying strongly influences the structure, dynamics, and glass forming ability of metallic supercooled liquids, Appl. Phys. Lett. **93**, 111913 (2008).

[42] X. Hui, H. Z. Fang, G. L. Chen, S. L. Shang, Y. Wang, and Z. K. Liu, Icosahedral ordering in $Zr_{41}Ti_{14}Cu_{12.5}Ni_{10}Be_{22.5}$ bulk metallic glass, Appl. Phys. Lett. **92**, 201913 (2008).

[43] S. G. Hao, C. Z. Wang, M. Z. Li, R. E. Napolitano, and K. M. Ho, Dynamic arrest and glass formation induced by self-aggregation of icosahedral clusters in $Zr_{1-x}Cu_x$ Alloys, Phys. Rev. B. **84**, 064203 (2011).

[44] K. N. Lad, N. Jakse, and A. Pasturel, Signatures of fragile-to-strong transition in a binary metallic glass-forming liquid, J. Chem. Phys. **136**, 104509 (2012).

[45] M. Lee, C. M. Lee, K. R. Lee, E. Ma, and J. C. Lee, Networked interpenetrating connections of icosahedra: Effects on shear transformations in metallic glass, Acta Mater. **59**, 159 (2011).

[46] M. Li, C. Z. Wang, S. G. Hao, M. J. Kramer, and K. M. Ho, Structural heterogeneity and medium-range order in Zr_xCu_{100-x} metallic glasses, Phys. Rev. B **80**, 184201 (2009).

[47] R. Soklaski, Z. Nussinov, Z. Markow, K. F. Kelton, and L. Yang, Connectivity of icosahedral network and a dramatically growing static length scale in Cu-Zr binary metallic glasses, Phys. Rev. B **87**, 184203 (2013).

[48] Z. W. Wu, M. Z. Li, W. H. Wang, and K. X. Liu, Correlation between structural relaxation and connectivity of icosahedral clusters in CuZr metallic glass-forming liquids, Phys. Rev. B **88**, 054202 (2013).

[49] C. Yang *et al.*, Splitting of fast relaxation in a metallic glass by laser shocks, Phys. Rev. B **109**, 024201 (2024).

[50] S. D. Feng, W. Jiao, S. P. Pan, L. Qi, W. Gao, L. M. Wang, G. Li, M. Z. Ma, and R. P. Liu, Transition from elasticity to plasticity in $Zr_{35}Cu_{65}$ metallic glasses: A molecular dynamics study, J. Non.-Cryst. Solids **430**, 94 (2015).

[51] S. D. Feng, K. C. Chan, L. Zhao, S. P. Pan, L. Qi, L. M. Wang, and R. P. Liu, Rejuvenation by weakening the medium range order in $Zr_{46}Cu_{46}Al_8$ metallic glass with pressure preloading: A molecular dynamics simulation study, Mater. Des. **158**, 248 (2018).

[52] G. Yang, L. Liu, J. Yi, J. Li, and L. Kong, Outside-in disintegration of medium-range order in nano metallic glasses during torsion deformation revealed by molecular dynamics simulations, J. Non.-Cryst. Solids **595**, 121827 (2022).

[53] M. Wakeda and Y. Shibutani, Icosahedral clustering with medium-range order and local elastic properties of amorphous metals, Acta Mater. **58**, 3963 (2010).

[54] J. Ding, Y. Q. Cheng, and E. Ma, Full icosahedra dominate local order in $Cu_{64}Zr_{34}$ metallic glass and supercooled liquid, Acta Mater. **69**, 343 (2014).

[55] C. Han, W. Yang, Y. Lan, and M. Sun, Al addition on the short and medium range order of CuZrAl metallic glasses, Physica B (Amsterdam, Neth.) **619**, 413237 (2021).

[56] Z.-Y. Yang, Y.-J. Wang, and L.-H. Dai, Hidden spatiotemporal sequence in transition to shear band in amorphous solids, Phys. Rev. Res. **4**, 023220 (2022).

[57] G. P. Shrivastav, P. Chaudhuri, and J. Horbach, Yielding of glass under shear: A directed percolation transition precedes shear-band formation, Phys. Rev. E **94**, 042605 (2016).

[58] P. Cao, K. A. Dahmen, A. Kushima, W. J. Wright, H. S. Park, M. P. Short, and S. Yip, Nanomechanics of slip avalanches in amorphous plasticity, J. Mech. Phys. Solids **114**, 158 (2018).

[59] S. Plimpton, Fast parallel algorithms for short-range molecular dynamics, J. Comput. Phys. **117**, 1 (1995).

[60] M. I. Mendelev, Y. Sun, F. Zhang, C. Z. Wang, and K. M. Ho, Development of a semi-empirical potential suitable for molecular dynamics simulation of vitrification in Cu-Zr alloys, J. Chem. Phys. **151**, 214502 (2019).

[61] M. Parrinello and A. Rahman, Polymorphic transitions in single crystals: A new molecular dynamics method, J. Appl. Phys. **52**, 7182 (1981).

[62] W. G. Hoover, Canonical dynamics: Equilibrium phase-space distributions, Phys. Rev. A **31**, 1695 (1985).

[63] S. Nosé, A unified formulation of the constant temperature molecular dynamics methods, J. Chem. Phys. **81**, 511 (1984).

[64] A. J. Cao, Y. Q. Cheng, and E. Ma, Structural processes that initiate shear localization in metallic glass, Acta Mater. **57**, 5146 (2009).

[65] Y. Fan, T. Iwashita, and T. Egami, How thermally activated deformation starts in metallic glass, Nat. Commun. **5**, 5083 (2014).

[66] J. C. Dyre, Solidity of viscous liquids. IV. Density fluctuations, Phys. Rev. E **74**, 021502 (2006).

[67] L. Wang, N. Xu, W. H. Wang, and P. Guan, Revealing the link between structural relaxation and dynamic heterogeneity in glass-forming liquids, Phys. Rev. Lett. **120**, 125502 (2018).

[68] W. Kob and H. C. Andersen, Testing mode-coupling theory for a supercooled binary Lennard-Jones mixture. II. Intermediate scattering function and dynamic susceptibility, Phys. Rev. E **52**, 4134 (1995).

[69] Y. Q. Cheng, H. W. Sheng, and E. Ma, Relationship between structure, dynamics, and mechanical properties in metallic glass-forming alloys, Phys. Rev. B **78**, 014207 (2008).

[70] D. Şopu, A. Stukowski, M. Stoica, and S. Scudino, Atomic-level processes of shear band nucleation in metallic glasses, Phys. Rev. Lett. **119**, 195503 (2017).

[71] M. L. Falk and J. S. Langer, Dynamics of viscoplastic deformation in amorphous solids, Phys. Rev. E **57**, 7192 (1998).

[72] N. A. Fleck and J. W. Hutchinson, Strain gradient plasticity, Adv. Appl. Mech. **33**, 295 (1997).

[73] P. Zhao, J. Li, and Y. Wang, Heterogeneously randomized STZ model of metallic glasses: Softening and extreme value statistics during deformation, Int. J. Plast. **40**, 1 (2013).

[74] Z. Y. Yang and L. H. Dai, Structural origin of deformation and dynamical heterogeneity in metallic glasses, Phys. Rev. Mater. **7**, 113601 (2023).